Journal of Materials Chemistry A

PAPER

View Article Online
View Journal | View Issue

Cite this: J. Mater. Chem. A, 2016, 4, 3754

Paper-based all-solid-state flexible micro-supercapacitors with ultra-high rate and rapid frequency response capabilities†

Wenwen Liu,[ab] Congxiang Lu,[a] Hongling Li,[a] Roland Yingjie Tay,[a] Leimeng Sun,[a] Xinghui Wang,[a] Wai Leong Chow,[a] Xingli Wang,[a] Beng Kang Tay,*[ac] Zhongwei Chen,*[b] Ji Yan,[b] Kun Feng,[b] Gregory Lui,[b] Ricky Tjandra,[b] Lathankan Rasenthiram,[b] Gordon Chiu[b] and Aiping Yu*[b]

Received 6th January 2016
Accepted 26th January 2016

DOI: 10.1039/c6ta00159a

www.rsc.org/MaterialsA

Paper-based flexible supercapacitors (SCs) have attracted great attention as they enable the realization of next-generation bendable, light-weight, and environmentally-friendly portable electronics. However, conventional paper-based SCs adopt a sandwich-like structure suffering from poor rate performance, slow frequency response and difficulty in direct integration with other micro-devices. We report here for the first time paper-based all-solid-state flexible planar micro-supercapacitors (MSCs) using poly(3,4-ethylenedioxythiophene):poly(styrene sulfonate) (PEDOT:PSS)-CNT/Ag as the electrode material by the inkjet printing technique. The as-fabricated paper-based all-solid-state flexible MSCs deliver the best rate capability among all reported paper-based MSCs/SCs (up to 10 000 mV s^{-1}), fast frequency response (relaxation time constant $\tau_0 = 8.5$ ms), high volumetric specific capacitance (23.6 F cm^{-3}) and long cycle stability (92% capacitance retention after 10 000 cycles), which shows a strong dependence on the film thickness and the interdigitated spacing between neighbouring fingers, respectively. Furthermore, the series and parallel connections reveal that the as-prepared paper-based MSCs obey the basic theorem of series and parallel connections of capacitors, respectively. The combination of the simple fabrication technology and excellent performances presented here not only make paper-based all-solid-state flexible MSCs an attractive candidate for powering future flexible portable electronics, but also provide important references for the design and fabrication of other high-performance flexible energy storage devices.

1. Introduction

Recently, the continuous developments in miniaturized wearable/portable electronics, implantable medical devices, and wireless sensor networks are driving an increasing demand for micro-scale, flexible, light-weight, cheap, sustainable and renewable power sources to build self-powered micro/nano-devices and systems.[1–5] The major bottleneck in this field is how to develop micro-scale energy storage devices with high power and energy densities, by rational design of the device architecture and structure of electrodes, using desirable electrode materials and scalable fabrication technologies.[5] Among the various energy storage devices, micro-supercapacitors (MSCs), especially flexible MSCs, have attracted tremendous attention as a promising candidate to satisfy requirements for today's portable microelectronic devices due to several unique advantages including high power density, long cycle life, flexibility, shape diversity and light-weight.[6–8]

One of the key challenges in fabricating flexible MSCs is to find bendable electrode materials with good mechanical properties and high electrochemical performance.[7–12] An effective and promising strategy is to integrate functional materials including carbonaceous materials, metal oxides/hydroxides and conductive polymers into various flexible substrates.[6,7,9,11,13–18] Among these, paper exhibits a set of properties that are different from those of conventional flexible substrates (*e.g.* PET, PDMS, and metal substrate) due to its natural features (such as the intrinsic porous surface and the large number of natural surface functional groups). Moreover, paper is also widely available, low-cost, recyclable, and environmentally friendly. These unique properties make paper very promising for the fabrication of thin, light-weight and flexible storage devices.[19–21] However, conventional paper-based flexible SCs adopt

[a]Novitas, Nanoelectronics Center of Excellence, School of Electrical and Electronic Engineering, Nanyang Technological University, Singapore 639798. E-mail: ebktay@ntu.edu.sg

[b]Department of Chemical Engineering, Waterloo Institute for Nanotechnology, University of Waterloo, Waterloo, Ontario N2L3G1, Canada. E-mail: zhwchen@uwaterloo.ca; aipingyu@uwaterloo.ca

[c]CINTRA CNRS/NTU/THALES, Nanyang Technological University, Singapore 637553

† Electronic supplementary information (ESI) available. See DOI: 10.1039/c6ta00159a

a sandwich-like structure suffering from poor rate performance, slow frequency response and difficulty in direct integration with other micro-devices. These properties are particularly important if the MSCs/SCs are to replace electrolytic capacitors in applications such as AC line-filtering, or if they are to be coupled with other energy storage devices to provide peak power. Additionally, the most popular micro-fabrication techniques (such as photolithography) in combination with deposition techniques (such as chemical vapour deposition and sputtering techniques) have been employed to build flexible MSCs.[22–26] However, most of the aforementioned techniques involve a complicated fabrication process, toxic chemicals, harsh fabrication conditions, and high cost, which can hardly be scaled up. Thus, it is still necessary to develop convenient, low-cost and scalable techniques to controllably prepare thin, flexible and nano-structured electrodes with high performance.

To this end, it still remains a big challenge to design and fabricate high-performance paper-based flexible planar MSCs with cost-effective materials by a simple and scalable fabrication process. In this work, we report here for the first time paper-based all-solid-state flexible planar MSCs using poly(3,4-ethylenedioxythiophene):poly(styrene sulfonate) (PEDOT:PSS)-CNT/Ag as the electrode material by the inkjet printing technique. First, inkjet printing technology is not only a simple, large-scale, low-cost and high-utilization method, but also allows for the precise control of the pattern geometry, location, thickness and uniformity of the electrode film.[27–32] In the electrode material design, we focus on the synergistic effects of the combination of PEDOT:PSS-CNTs, Ag nano-particles and the paper substrate to effectively take advantage of each component. The unique 3D porous structure formed in the PEDOT:PSS-CNT/Ag composite film is beneficial for effective electrolyte transport and active-site accessibility. Furthermore, the highly conductive PEDOT:PSS-CNT/Ag composite film can directly act as both electrode and current collector without using an additional conductive material, decreasing the weight of the device. As expected, the as-prepared paper-based all-solid-state flexible MSCs deliver the best rate capability among all reported paper-based MSCs/SCs (up to 10 000 mV s^{-1}), fast frequency response (relaxation time constant $\tau_0 = 8.5$ ms), high volumetric specific capacitance (23.6 F cm^{-3}) and long cycle stability (92% of capacitance retention after 10 000 cycles), which show a strong dependence on the film thickness and the interdigitated spacing between neighbouring fingers, respectively. Furthermore, the serial and parallel tests confirm that the as-prepared paper-based MSCs obey the basic theorem of series and parallel connections of capacitors, respectively. The combination of excellent electrochemical performance and scalable fabrication technology of paper-based MSCs provide a new way for the development of next-generation portable electronics.

2. Experimental

2.1 Materials

PEDOT:PSS-CNT and conductive Ag inks were purchased from Poly-Ink Company and were sonicated for 10 min before using. Inkjet photo paper was chosen as a flexible substrate, and its corresponding physical/chemical properties are shown in Fig. S1.† All other chemicals were directly used as-received.

2.2 Design and fabrication of paper-based PEDOT:PSS-CNT/Ag MSCs

Inkjet printing was performed using a Dimatix DMP-2800 inkjet printer (Fig. S2†). This inkjet printer utilizes 16 micro-fabricated piezoelectric nozzles for on-demand and programmable generation of 10 picoliter microscopic ink droplets. All of inkjet printing experiments were performed at room temperature.

The detailed processes for the preparation of paper-based PEDOT:PSS-CNT/Ag MSCs were as follows. First, the interdigitated electrode patterns were designed using the software that was provided alongside the inkjet printer. Next, PEDOT:PSS-CNT ink was printed on photo paper with the designed structure to form a PEDOT:PSS-CNT film followed by drying at 200 °C for 10 min under vacuum. Subsequently, Ag ink was overprinted on the surface of the PEDOT:PSS-CNT film using the same designed pattern. After the inkjet printing process, the samples were dried under vacuum at 80 °C for 2 h. Finally, the fabricated MSCs were obtained by drop-casting the PVA/H_3PO_4 electrolyte followed by drying in air. Additionally, to reveal the effects of the film thickness and electrode structure on the electrochemical performance of MSCs, MSCs with different numbers of PEDOT:PSS-CNT film layers (1, 5 and 10 layers) and different interdigitated spacings (600, 900 and 1200 μm) were fabricated, respectively.

2.3 Morphological and structural characterization

A field emission scanning electron microscope (FESEM, LEO 1550 GEMINI) was employed to study the morphologies of the as-prepared samples. Transmission electron microscopy (TEM) and high resolution TEM (HRTEM) were carried out using a JEOL JEM-2100F. Raman measurements were conducted using a WITecCRM200 Raman system with a 532 nm laser as the excitation source. The thickness of the hybrid film was determined using a Bruker Dektak XT surface profiler. The conductivity of the as-prepared PEDOT:PSS-CNT film was measured by the four-probe method.

2.4 Electrochemical measurement

All electrochemical measurements were carried out in a two-electrode system using an Autolab workstation (PGSTAT302N) at room temperature. Galvanostatic charge/discharge tests were measured with a constant current density of 0.25 mA cm^{-2}. Electrochemical impedance spectroscopy (EIS) tests were performed using a frequency ranging from 100 kHz to 0.05 Hz at open circuit potential with an AC perturbation of 5 mV. Cyclic voltammetry (CV) tests were carried out at different scan rates ranging from 10 to 50 000 mV s^{-1} with a potential window from 0 to 0.9 V. Capacitance values were calculated from the CV curves by the equation:

$$C_{\text{device}} = \frac{1}{\nu(V_{\text{f}} - V_{\text{i}})} \int_{V_{\text{i}}}^{V_{\text{f}}} I(V)\mathrm{d}V \quad (1)$$

The specific capacitances were calculated based on the volume of the device stack according to the following equation:

$$C_{\text{stack}} = \frac{C_{\text{device}}}{V} \quad (2)$$

where ν is the scan rate (mV s^{-1}), V_f and V_i are the potential limits of the voltammetric curve, $I(V)$ is the voltammetric discharge current (A), C_{device} is the capacitance contribution from hybrid films (F cm^{-2}), and C_{stack} is the volumetric stack capacitance of the device (F cm^{-3}). The volumetric stack capacitances were calculated by taking into account the whole volume of the device including the volume of hybrid film electrodes and the interspaces between the electrodes.

Additionally, the energy density (E) and power density (P) were calculated using the following equations, respectively:

$$E = \frac{C_{\text{stack}} \times \Delta V^2}{7200} \quad (3)$$

$$P = \frac{E \times 3600}{t} \quad (4)$$

where C_{stack} is the volumetric stack capacitance (F cm^{-3}), ΔV is the operating potential window (V), Δt is the discharge time (s), E is the energy density (Wh cm^{-3}) and P is the power density (W cm^{-3}).

3. Results and discussion

SEM and TEM were used to characterize the morphology and structure of PEDOT:PSS-CNT and Ag nano-particle inks. As the dispensed ink dries, the PEDOT:PSS-CNTs entangle and interconnect with each other (Fig. 1a), which could be beneficial for

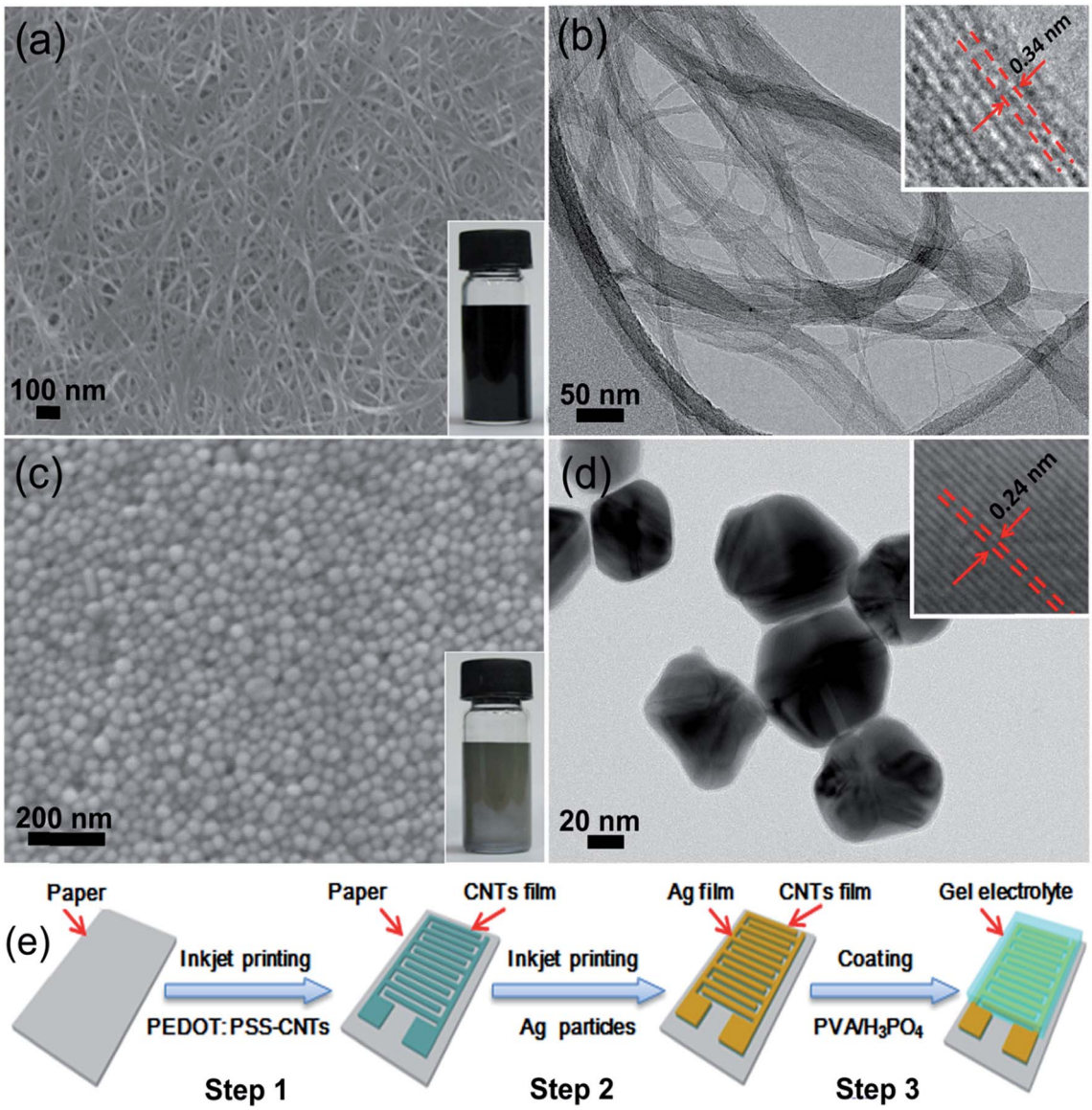

Fig. 1 (a) Top-view SEM and (b) TEM images of PEDOT:PSS-CNT ink. The inset in (a) is a digital photograph of PEDOT:PSS-CNT ink. (c) Top-view SEM and (d) TEM images of Ag ink. The inset in (c) is the digital photograph of Ag ink. (e) Schematic illustrations of the fabrication process of paper-based all-solid-state flexible MSCs.

the transfer of electrons. The TEM image (Fig. 1b) shows the PEDOT:PSS-CNTs with lengths ranging from 0.3 to 1.6 μm and diameters ranging from 0.5 to 3.2 nm. Good mono-dispersity and relative narrow size distribution of the Ag nano-particles can be observed from the representative SEM image (Fig. 1c). Their corresponding TEM image (Fig. 1d) reveals their fivefold twinning structure with a lattice-fringe spacing of 0.24 nm (inset in Fig. 1d) corresponding to the (111) planes of Ag.[33] As shown in the insets of Fig. 1a and c, the PEDOT:PSS-CNT and Ag nano-particle inks exhibit high stability without any noticeable precipitation after one month indicating the long-term stability. Here, based on the abovementioned PEDOT:PSS-CNT and Ag nano-particle inks, paper-based MSCs are successfully designed and built by the inkjet printing technique (Fig. 1e). The detailed fabrication processes are described in the Experimental section.

The optical images of the as-fabricated paper-based MSCs are shown in Fig. 2a. The interdigitated fingers show a blue-grey color after being printed with the PEDOT:PSS-CNT ink. Afterward, the blue-grey colored interdigitated fingers turned silver-gray, demonstrating the successful overprinting of a nano-silver layer. The low magnification top-view SEM image (Fig. 2b) shows the interdigitated PEDOT:PSS-CNT/Ag composite film electrodes with a smooth surface and highly regulated size and structure. This is direct evidence for one of the advantage of inkjet printing, allowing efficient and accurate control of the interdigitated electrode structure. The high magnification top-view SEM image (Fig. 2c) reveals that PEDOT:PSS-CNTs are tangled and twisted with each other, forming a uniform 3D network film on the paper substrate. Note that the porous structure is still retained after the overprinting of Ag film on the

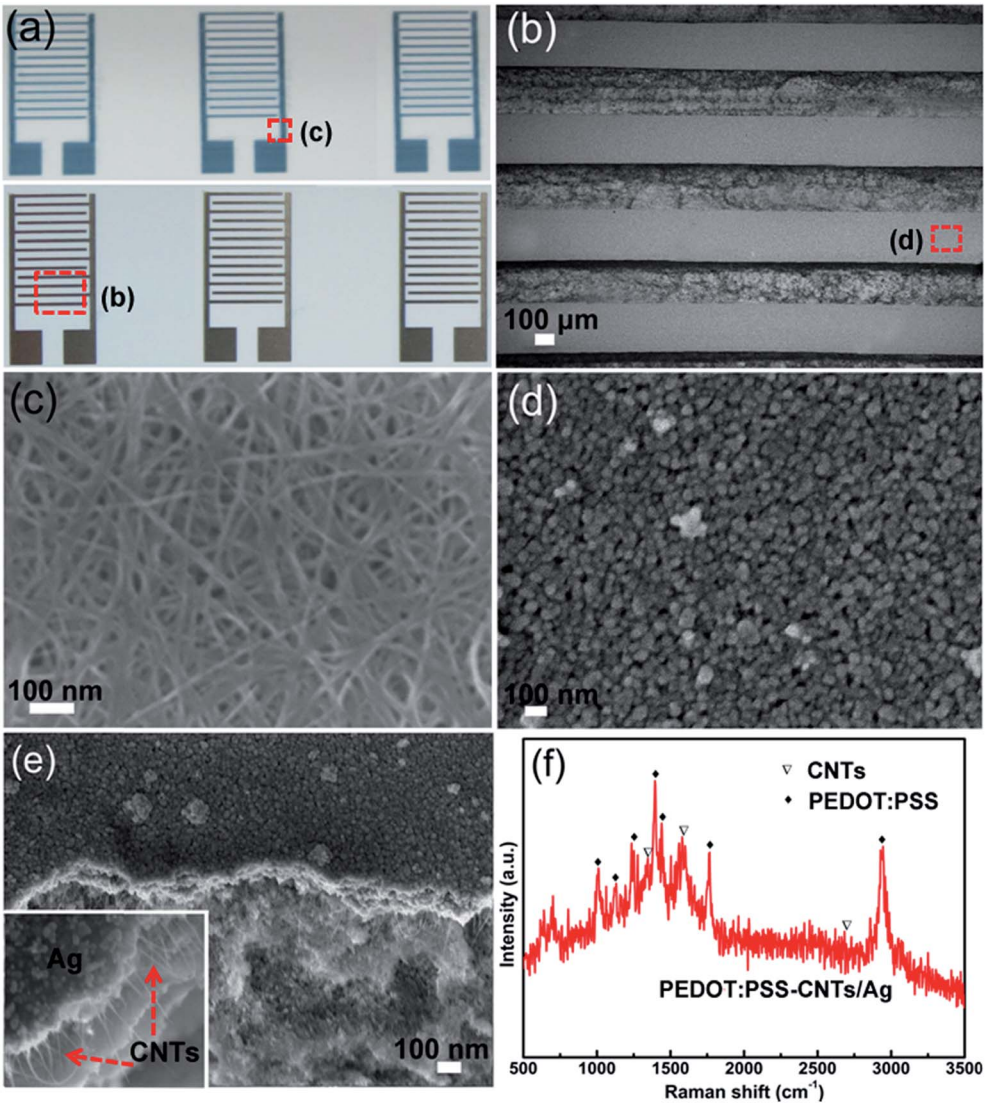

Fig. 2 (a) Optical images of MSCs with the interdigitated PEDOT:PSS-CNT film before (top) and after (bottom) overprinting of the Ag film. (b) Low magnification top-view SEM image of an interdigitated electrode based on the PEDOT:PSS-CNT/Ag composite film located in panel (a). (c) High magnification top-view SEM image of the PEDOT:PSS-CNT film located in panel (a). (d) High magnification top-view SEM image of the Ag film located in panel (b). (e) Cross-sectional SEM image of the interdigitated PEDOT:PSS-CNT/Ag composite film printed on paper. (f) Raman spectrum of the PEDOT:PSS-CNT/Ag film.

surface of the PEDOT:PSS-CNT film (Fig. 2d). Here, Ag nanoparticles act as a conductive bridge which enables the formation of more efficient electron-transport channels, thereby further improving the conductivity of the PEDOT:PSS-CNT film. The unique 3D porous structure formed in the PEDOT:PSS-CNT/Ag composite film is beneficial for effective electrolyte transport and active-site accessibility. Furthermore, the highly conductive PEDOT:PSS-CNT/Ag composite film can directly act as both electrode and current collector without using an additional conductive material, decreasing the weight of the device. The cross-sectional SEM image (Fig. 2e) confirms that no PEDOT:PSS-CNT/Ag penetrates into the paper membrane, which avoids short circuiting of the MSCs. The Raman spectrum of the PEDOT:PSS-CNT/Ag composite film (Fig. 2f) shows two prominent peaks at 1360 and 1583 cm^{-1} corresponding to the well-documented D and G bands of CNTs,[34] respectively, and a series of other characteristic peaks can be indexed to PEDOT:PSS.[35] These characterization results indicate that the PEDOT:PSS-CNT/Ag composite film has been successfully printed on the paper substrate using the inkjet printing technique. The mechanical adhesion between the PEDOT:PSS-CNT/Ag film and paper substrate is evaluated by performing a "Scotch Tape test", as shown in Fig. S3.† No obvious PEDOT:PSS-CNT/Ag film is observed on the tape after the test,

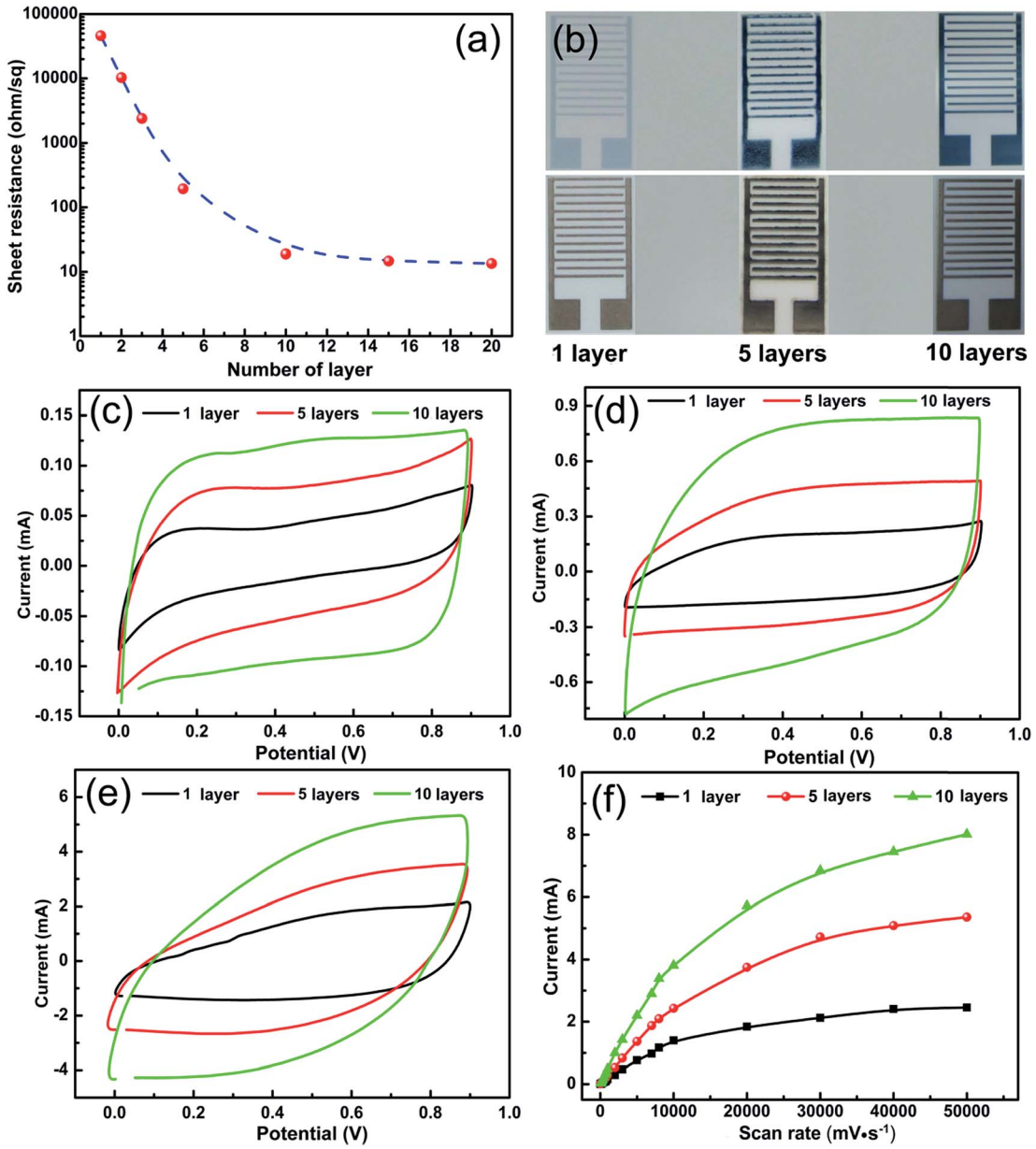

Fig. 3 (a) Variation of sheet resistance with different numbers of printing layers of PEDOT:PSS-CNT films. (b) Optical image of the fabricated paper-based MSCs with different numbers of PEDOT:PSS-CNT film layers before (top) and after (bottom) overprinting of Ag ink. CV curves of MSCs with different numbers of PEDOT:PSS-CNT film layers at different scan rates: (c) 100 mV s^{-1}, (d) 1000 mV s^{-1}, (e) 10 000 mV s^{-1}, respectively. (f) Evolution of the corresponding discharge current *versus* scan rate for paper-based MSCs with different numbers of PEDOT:PSS-CNT film layers.

demonstrating that the PEDOT:PSS-CNT/Ag film strongly binds onto the paper substrate. As mentioned above, porous structure, good mechanical property and strong adhesion make the binder-free paper-based MSCs suitable for application in flexible energy storage devices.

The electrical properties exhibit an obvious thickness dependence when nano-structured films become thin.[36] Meanwhile, the electronic conductivity of an electrode material plays a vital role in the electrochemical performance. These facts inspire us to think whether it is possible to control the electrochemical performance of paper-based MSCs by adjusting the thickness of PEDOT:PSS-CNT films or not. The sheet resistances of PEDOT:PSS-CNT films with various numbers of film layers are plotted in Fig. 3a. It is observed that with the increase in the deposition amount of CNTs, the sheet resistances of PEDOT:PSS-CNT films continue to decrease rapidly until reaching 10 layers (almost 4 orders of magnitude variation). Beyond this point the sheet resistances are relatively invariant to further increases of the film layers, indicating that the sheet resistances of the PEDOT:PSS-CNT films show a strong dependence on the film thickness.[37,38] Such a pronounced change in the value of the conductivity may have a significant effect on their electrochemical performance. Therefore, better understanding of how the PEDOT:PSS-CNT films' thicknesses affect their electrochemical performance will be of great significance and may provide important insights into the design and preparation of film-based energy storage devices. To reveal the effect of the thicknesses of PEDOT:PSS-CNT films on the electrochemical performance of MSCs, paper-based MSCs with different layer numbers of PEDOT:PSS-CNT films (1 layer, 5 layers and 10 layers) are fabricated (Fig. 3b) and the corresponding thicknesses of composite films are shown in Fig. S4.† Here, all other parameters (including the width of the finger, the length of the finger, the width of the interdigitated spacing between the adjacent fingers, the thickness of the Ag film and the total surface of the cell) were kept constant (Fig. S5†).

Cyclic voltammetry (CV) measurements were firstly performed to evaluate the effect of the thickness of PEDOT:PSS-CNT films on the electrochemical performance of paper-based all-solid-state flexible MSCs. The CV curves (Fig. 3c and d) exhibit a nearly rectangular shape and rapid current response on voltage reversal at each end potential at low scan rates, indicative of near-ideal capacitive behavior.[8,39,40] Importantly, the CV curves still retain a good rectangular shape even at an ultra-high scan rate of 10 000 mV s^{-1} (Fig. 3e), demonstrating quick charge/discharge propagation in the PEDOT:PSS-CNT/Ag composite film and ultra-high rate capability of paper-based MSCs.[39,40] To the best of our knowledge, the paper-based all-solid-state flexible MSCs presented here deliver the best rate capability among all reported paper-based MSCs/SCs.[4,17,20,28,30,31] Meanwhile, such excellent rate performance is comparable to those of reported non-paper-based MSCs using other active materials including carbide-derived carbon,[24] onion-like carbon,[22] reduced graphene oxide,[7,8,10,12] graphene/CNTs,[25,41,42] graphene/polyaniline,[23] and graphene/MnO_2.[39] The in-depth study of the relationship between the current responses of MSCs with different thicknesses of PEDOT:PSS-CNT films and the scan rates are shown in Fig. 3f. Notably, the current values slowly deviate from the linear region at ultra-high scan rates due to the limited ion diffusion,[6,7,26,43–45] but a linear dependence of the discharge currents on the scan rates is recognized at least up to 8000 mV s^{-1}, further revealing the excellent rate capability of paper-based MSCs. In addition, it can also be observed that at a constant scan rate, the thicker the PEDOT:PSS-CNT film, the larger the discharge current response. This is because more active materials have been deposited and a larger number of PEDOT:PSS-CNT network interconnections have been formed when the layers are increased, which enhances the current response.

To gain more insight into the effects of the thicknesses of PEDOT:PSS-CNT films on the electrochemical performance of paper-based MSCs, the volumetric specific capacitance, the galvanostatic charge/discharge (GCD) curves and Nyquist plots are shown in Fig. 4. As reported, the volumetric capacitance gives a more accurate evaluation of the true performance of a supercapacitor, especially for MSCs due to the small active material mass-loading.[7,8,10,17,41] Therefore, all of the specific capacitance values of the MSCs in this work is calculated based on the volume of the stack, if not otherwise specified. As displayed in Fig. 4a, the volumetric specific capacitances of the paper-based MSCs decrease with the increase of scan rates ranging from 10 to 50 000 mV s^{-1}, which is attributed to the insufficient time available for ion diffusion and adsorption in the inside of PEDOT:PSS-CNT/Ag films.[12,46] At a fixed scan rate, the volumetric specific capacitance of paper-based MSCs displays a downward trend with increasing number of film layers (from 1 to 10 layers), while the area specific capacitance shows the upward trend (Fig. S6†). This can be explained by the following reason: increasing the number of film layers can improve the electronic conductivity of the film and increase the mass-loading of active materials, which has the positive contribution to the area specific capacitance. However, increasing the number of film layers also results in the increase of the diffusion resistance of electrolyte penetration into the inner film structure, thus reducing the utilization of active materials and reducing the overall electrochemical performance of the MSCs. The highest volumetric specific capacitance of 23.6 F cm^{-3} for the paper-based MSCs (1 layer of the PEDOT:PSS-CNT film) is obtained at a scan rate of 10 mV s^{-1}, which is better or at least comparable with those of reported paper- and non-paper-based MSCs using other electrode materials such as reduced graphene films (17.5 F cm^{-3}),[7] polypyrrole (11.0 F cm^{-3}),[20] active carbon (9.00 F cm^{-3}),[22] MnO_2/onion-like carbon (7.04 F cm^{-3}),[30] laser reduction graphene (3.10 F cm^{-3}),[8] onion-like carbon (1.10 F cm^{-3})[22] and graphene/CNTs (1.08 F cm^{-3}).[25] To further demonstrate this point, a Ragone plot showing the volumetric energy density with respect to the volumetric power density is plotted in Fig. S7.† The as-fabricated paper-based MSCs exhibit a maximum volumetric energy density of 42.1 mW h cm^{-3} (at a power density of 89.1 mW cm^{-3}), which is higher than those of recently reported paper-based MSCs/SCs using other electrode materials such as polypyrrole,[20] multi-walled carbon nanotube/Ag nanoparticle,[28] MnO_2/onion-like carbon[30] and graphite/polyaniline networks.[47]

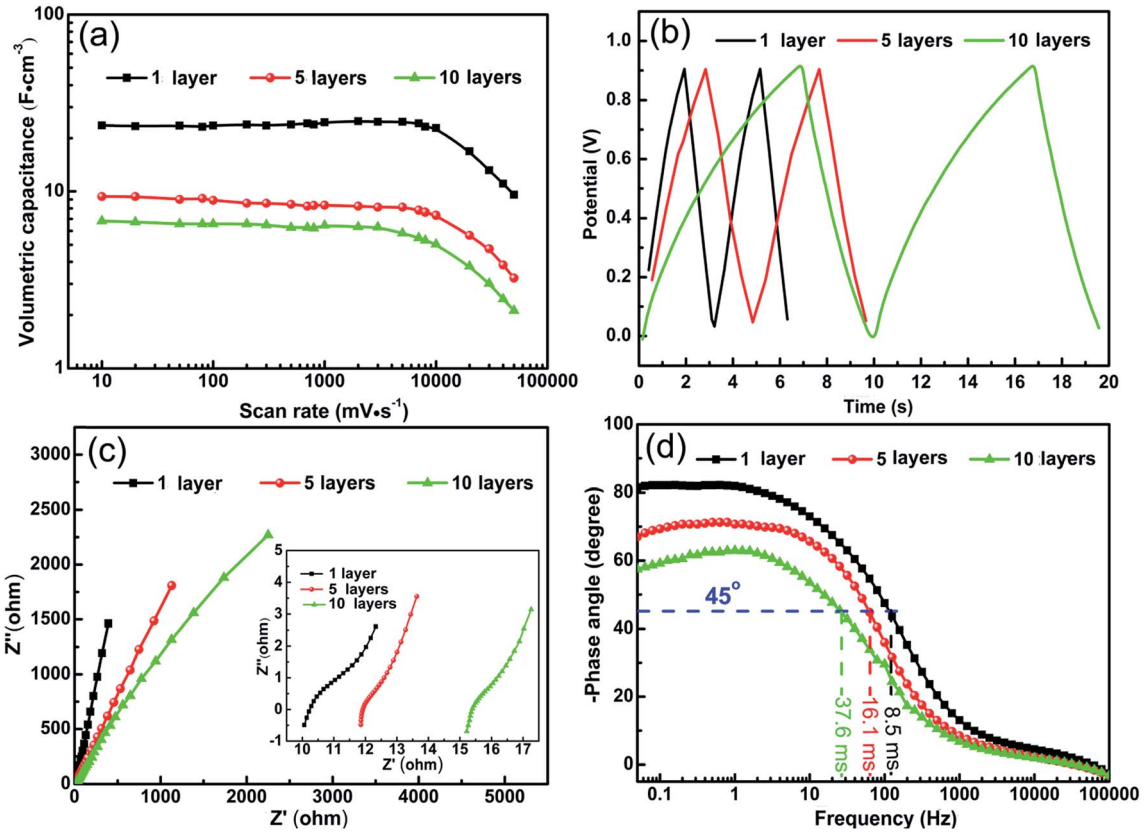

Fig. 4 Electrochemical performance of paper-based MSCs with different numbers of deposited layers: (a) evolution of the volumetric capacitance *versus* scan rate, (b) galvanostatic charge–discharge (GCD) curves in the voltage range between 0 and 0.9 V at a fixed current density of 0.25 mA cm^{-2}, (c) Nyquist plots with a frequency range from 100 kHz to 0.05 Hz using a perturbation amplitude of 5 mV at the open circuit potential (inset shows an enlarged curve in the high-frequency region), and (d) impedance phase angle as a function of frequency ranging from 100 kHz to 0.05 Hz.

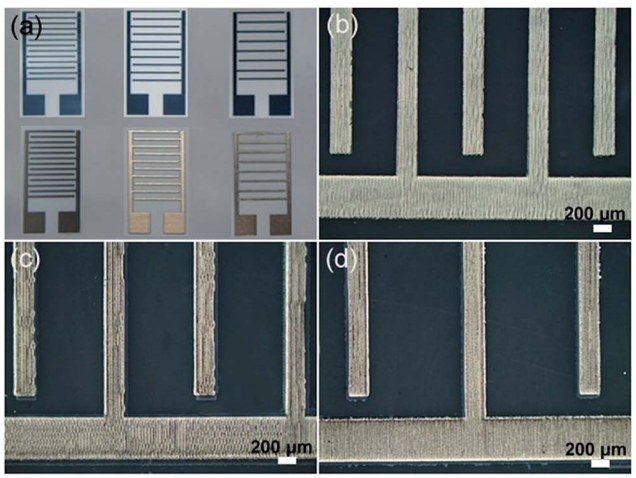

Fig. 5 (a) Optical images of paper-based PEDOT:PSS-CNT/Ag MSCs with different interdigitated spacings between the adjacent fingers before (top) and after (bottom) overprinting of Ag ink. Optical images of (b) MSCs (600 μm), (c) MSCs (900 μm), and (d) MSCs (1200 μm), respectively.

Meanwhile, their performance is also better than or comparable to those of reported non-paper-based MSCs.[8,10,25,41,42,48] Encouragingly, these energy density values are at least two orders of magnitude higher than those of commercial electrolytic capacitors (3 V/300 μF),[8,10] and even comparable to those of the thin-film lithium batteries (4 V/500 μA h).[22] The excellent performance of paper-based MSCs is mainly contributed by the PEDOT:PSS-CNT/Ag hybrid film due to the synergistic effect of each component and the unique 3D porous structure of the film which provides a large surface area and decreases the ion diffusion resistance of the electrolyte on the electrode surface. Furthermore, all GCD curves of paper-based MSCs (Fig. 4b) exhibit a nearly ideal triangular shape and no obvious voltage drop appeared at the beginning of each discharge curve indicating ideal capacitive behaviour and relatively low resistance.[40,43] The discharge time increases with the number of printed layers at constant current densities, demonstrating a thickness dependence consistent with the data obtained from the CV curves. In addition, self-discharge curves of the MSCs reveal the relatively low self-discharge characteristics (Fig. S8†).

Electrochemical impedance spectra (EIS) of the paper-based MSCs with different numbers of PEDOT:PSS-CNT films are presented in Fig. 4c. All of Nyquist plots exhibit a very small semicircle in the high frequency range followed by a transition to linearity in the low frequency range, indicating good electrical conductivity and fast ion diffusion in the PEDOT:PSS-CNT

film.[7,40,49,50] Notably, MSCs with thin PEDOT:PSS-CNT films (1 layer) shows a smaller equivalent series resistance, mainly attributed to the shorter ion diffusion pathway. For a more informative analysis of EIS, the dependence of the phase angle on the frequency is plotted in Fig. 4d. The characteristic frequency (f_0) at the phase angle of 45° is 118.1 Hz for MSCs (1 layer), 62.1 Hz for MSCs (5 layers) and 26.6 Hz for MSCs (10 layers), corresponding to the relaxation time constant ($\tau_0 = 1/f_0$) of 8.50, 16.1 and 37.6 ms, respectively. The characteristic frequency (f_0) marks the point at which the resistive and capacitive impedances are equal, and at frequencies higher than f_0 the supercapacitors show more resistive behaviour.[17,41] The corresponding relaxation time constant (τ_0) is the minimum time needed to discharge all the energy from the device with an efficiency of greater than 50%.[17,41] The Nyquist plot shows that as the film thickness increases, so does the pore length (the distance that ions need to travel during the charge/discharge process) and subsequently the relaxation time constant. The relaxation time constants (τ_0) presented here are very promising compared with previously reported values for MSCs based on other materials such as reduced graphene films ($\tau_0 = 0.28$ ms),[7] laser reduction graphene ($\tau_0 = 19$ ms),[8] activated carbon ($\tau_0 = 700$ ms),[22] onion-like carbon ($\tau_0 = 26$ ms),[22] and graphene/CNT composites ($\tau_0 = 3.4$ ms).[25] Based on the above discussion and analysis, the number of film layers is proportional to the area specific capacitance and inversely proportional to the volumetric specific capacitance in paper-based MSCs. Therefore, depending on the chosen application the number of film layers can be adjusted to provide either a larger volumetric specific capacitance or larger area specific capacitance. It is also demonstrated that increasing the number of film layers increases the relaxation time constant.

The electrode structure is another highly important factor that affects the electrochemical performance of MSCs. Therefore, the effects of the interdigitated spacing between the adjacent fingers on the electrochemical performance of paper-based MSCs are systemically investigated in this work. Here, paper-based all-solid-state flexible MSCs with three different interdigitated spacing values (600, 900 and 1200 μm) were built (Fig. 5). Except for the interdigitated spacing between the adjacent fingers, all other parameters were kept constant (Fig. S9†). The CV curves of paper-based MSCs with different interdigitated spacings between the adjacent fingers are shown in Fig. 6a–c. The CV curves exhibit a quasi-rectangular shape even at a high scan rate of 1000 mV s^{-1}, indicating a near-ideal capacitive behavior.[10,39,43,44] The area under the CV curves decreases with increase of the interdigitated spacing between the adjacent fingers at a fixed scan rate, revealing an inverse

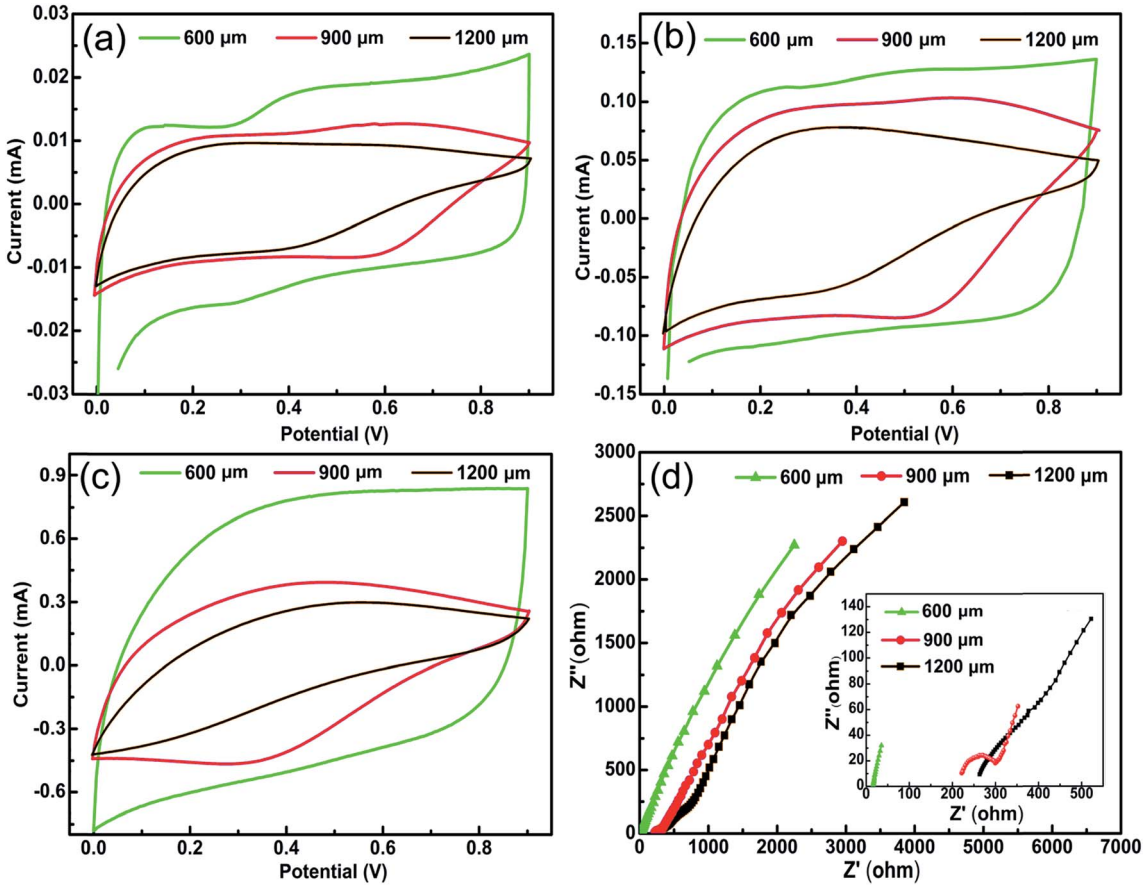

Fig. 6 CV curves of paper-based MSCs with different interdigitated spacing values between the adjacent fingers at different scan rates: (a) 10 mV s^{-1}, (b) 100 mV s^{-1}, (c) 1000 mV s^{-1}, respectively. (d) The corresponding Nyquist plots with a frequency range from 100 kHz to 0.05 Hz using a perturbation amplitude of 5 mV at the open circuit potential. The inset shows an enlarged curve in the high-frequency region.

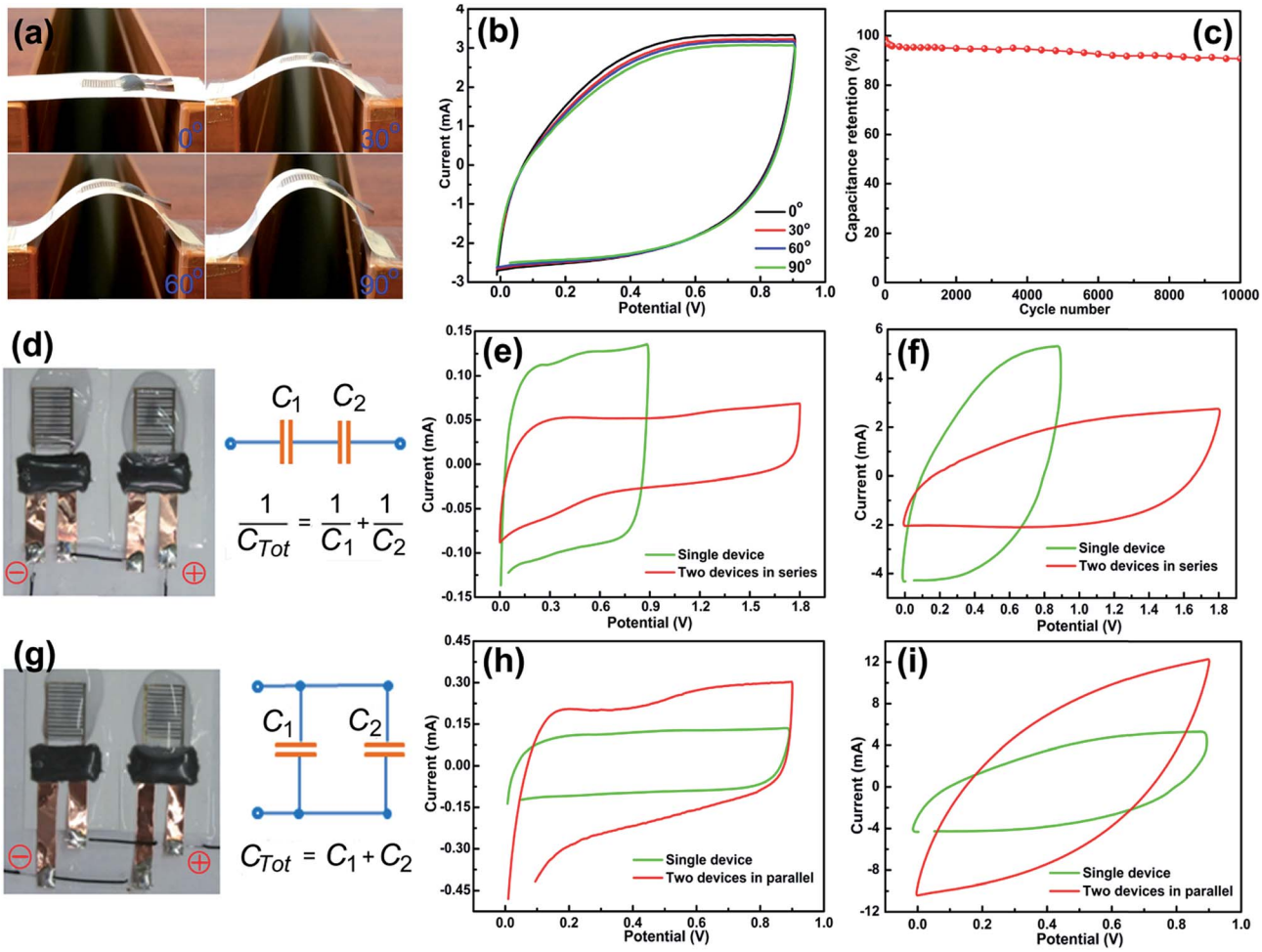

Fig. 7 (a) Optical images of paper-based MSCs bent at different angles. (b) CV curves of paper-based MSCs bent at different angles at 5000 mV s^{-1}. (c) Cycle stability of paper-based MSCs at 5000 mV s^{-1}. (d) Optical images and circuit diagram of two devices connected in series. CV curves of a single device and two devices connected in series at different scan rates: (e) 100 mV s^{-1}, (f) 10 000 mV s^{-1}, respectively. (g) Optical images and circuit diagram of two devices connected in parallel. CV curves of a single device and two devices connected in parallel at different scan rates: (h) 100 mV s^{-1}, (i) 10 000 mV s^{-1}, respectively.

relationship between the capacitance and the interdigitated spacing between adjacent fingers. To highlight the effects of the interdigitated spacing between the adjacent fingers on the electrochemical performance of the MSCs, the corresponding Nyquist plots are presented in Fig. 6d. The paper-based MSCs with large interdigitated spacing between the adjacent fingers increasingly diverges from the ideal capacitor behavior, suffering from higher ionic impedance and possessing lower phase angles in the low frequency regions which is due to ion diffusion limitations (Fig. S10†). Additionally, the time constant of MSCs (600 μm) is calculated to be 37.6 ms, in comparison to 990.1 ms for the MSCs (900 μm) and 5263.1 ms for the MSCs (1200 μm), suggesting that devices with smaller interdigitated spacing have faster frequency response capabilities. According to the above results and analysis, it can be concluded that the smaller the interdigitated spacing the MSCs has, the better performance they will have. A smaller interdigitated spacing will reduce the transport path of ions from one electrode to the counter electrode, resulting in a reduction of the internal resistance, complete utilization of active materials, and improvement of the rate capability.

When real applications are considered, flexibility is a must-have requirement for MSCs that are used to power flexible devices. Therefore, it is necessary to evaluate the capacitive performance of the paper-based MSCs under mechanical strain (Fig. 7a). The CV curves at different bending angles vary slightly (Fig. 7b), demonstrating excellent flexibility of paper-based MSCs used as a flexible power source. The durable capacitive performance is attributed to the good adhesion of the active material on the paper substrate and the "adhesive" effect of the gel electrolyte that maintains the integrity of the electrode components. The cycling stability of the paper-based MSCs is carried out by repeating the CV test in the potential window of 0 to 0.9 V at a scan rate of 5000 mV s^{-1}. The as-prepared paper-based MSCs still show 92% capacitance retention after 10 000 cycles (Fig. 7c), indicating a good cycle stability. Connecting the MSCs in series or parallel to increase the operating voltage or the current is required. Thus, the electrochemical performance

of a set of series- and parallel-connected MSCs were evaluated using CV. In the series connection (Fig. 7d), the voltage window can be broadened from 0.9 V for a single MSC to 1.8 V for two series-connected MSCs (Fig. 7e), which roughly conforms to the theorem of series connections of capacitors. Note that the CV curve of two series-connected MSCs still retains a quasi-rectangular shape even at an ultra-high scan rate of 10 000 mV s^{-1} (Fig. 7f). In the parallel case (Fig. 7g), the CV curve of two parallel-connected MSCs also retains the relative rectangular shape even at very high scan rates and the corresponding area under the CV curve is almost twice that of single MSCs (Fig. 7h and i), which is also in agreement with the rule. Thus it can be seen that the series and parallel connections of two paper-based MSCs obey the basic rule of series and parallel connections for capacitors. These results also reveal that the dimensional and physicochemical properties are highly consistent for each single MSC, and that inkjet printing is a facile, practical and scalable technique for the fabrication of MSCs.

4. Conclusion

In summary, we have successfully developed novel type paper-based all-solid-state flexible MSCs using the PEDOT:PSS-CNT/Ag hybrid film as the electrode material by the inkjet printing technique, which consist of a 3D PEDOT:PSS-CNT network and a high conductivity Ag film. In this structure, the PEDOT:PSS-CNT/Ag film not only directly acts as both the electrode and current collector, but also contributes to the overall capacitance. In addition, PEDOT:PSS-CNT/Ag is beneficial for building the binder-free electrode and decreasing the weight of the device. Overall, this unique combination of composite materials forming a 3D porous structure facilitates electrolyte transport and active-site accessibility, which make it a promising electrode material. Encouragingly, the novel structural design offers the paper-based all-solid-state flexible MSCs an ultra-high rate capability (up to 10 000 mV s^{-1}), rapid frequency response (a very short relaxation time constant, $\tau_0 = 8.5$ ms), high volumetric specific capacitance (23.6 F cm^{-3}) and long-term cycle stability (92% of the initial capacitance after 10 000 cycles). This excellent performance of paper-based all-solid-state flexible MSCs is mainly attributed to the synergistic effects from the combination of PEDOT:PSS-CNTs, Ag nano-particles and the paper substrate. Furthermore, the results also reveal that the electrochemical performance of paper-based all-solid-state flexible MSCs shows strong dependence on the thickness of the PEDOT:PSS-CNT film and the interdigitated spacing between neighbouring fingers. In all, our work presented here is not only a useful reference for the design and fabrication of other energy storage devices, but also supplies the best electrode materials so far and fully demonstrates the feasibility of printable MSCs using the inkjet technique.

Contributions

B. K. Tay, Z. W. Chen and A. P. Yu proposed and supervised the project. W. W. Liu, C. X. Lu, B. K. Tay and A. P. Yu designed the experiments. W. W. Liu, H. L. Li, R. Y. Tay, W. L. Chow, X. L. Wang, K. Feng, J. Yan, L. Rasenthiram and G. Chiu carried out the characterization of the related materials. W. W. Liu, H. L. Li, L. M. Sun, X. H. Wang, G. Lui and R. Tjandra performed the device assembly and electrochemical characterization. W. W. Liu, K. Feng, B. K. Tay, Z. W. Chen and A. P. Yu analyzed the data and wrote the paper. All authors discussed the results and commented on the manuscript.

Competing financial interests

The authors declare no competing financial interests.

Acknowledgements

The authors greatly appreciate the help of Prof. Qing Zhang and Dr Sebastien Pacchini and financial support from MOE Academic Research Fund (AcRF) RG81/12 project as well as Natural Sciences and Engineering Research Council of Canada.

References

1 M. Beidaghi and Y. Gogotsi, *Energy Environ. Sci.*, 2014, **7**, 867–884.
2 S. H. Li, D. K. Huang, B. Y. Zhang, X. B. Xu, M. K. Wang, G. Yan and Y. Shen, *Adv. Energy Mater.*, 2014, **4**, 1301655–1301661.
3 Y.-Z. Zhang, Y. Wang, T. Cheng, W.-. Lai, H. Pang and W. Huang, *Chem. Soc. Rev.*, 2015, **44**, 5181–5199.
4 V. L. Pushparaj, M. M. Shaijumon, A. Kumar, S. Murugesan, L. Ci, R. Vajtai, R. J. Linhardt, O. Nalamasu and P. M. Ajayan, *Proc. Natl. Acad. Sci. U. S. A.*, 2007, **104**, 13574–13577.
5 X. F. Wang, X. H. Lu, B. Liu, D. Chen, Y. X. Tong and G. Z. Shen, *Adv. Mater.*, 2014, **26**, 4763–4782.
6 Z.-S. Wu, K. Parvez, A. Winter, H. Vieker, X. J. Liu, S. Han, A. Turchanin, X. L. Feng and K. Müllen, *Adv. Mater.*, 2014, **26**, 4552–4558.
7 Z.-S. Wu, K. Parvez, X. L. Feng and K. Müllen, *Nat. Commun.*, 2013, **4**, 2487–2494.
8 M. F. EI-Kady and R. B. Kaner, *Nat. Commun.*, 2013, **4**, 1475–1483.
9 J. Feng, X. Sun, C. Z. Wu, L. L. Peng, C. W. Lin, S. L. Hu, J. L. Yang and Y. Xie, *J. Am. Chem. Soc.*, 2011, **133**, 17832–17838.
10 M. F. El-Kady, V. Strong, S. Dubin and R. B. Kaner, *Science*, 2012, **335**, 1326–1330.
11 C. Meng, J. Maeng, S. W. M. John and P. P. Irazoqui, *Adv. Energy Mater.*, 2014, **4**, 1301269–1301275.
12 Z. Q. Niu, L. Zhang, L. L. Liu, B. W. Zhu, H. B. Dong and X. D. Chen, *Adv. Mater.*, 2013, **25**, 4035–4042.
13 K. Jost, C. R. Perez, J. K. McDonough, V. Presser, M. Heon, G. Dion and Y. Gogotsi, *Energy Environ. Sci.*, 2011, **4**, 5060–5067.
14 L. B. Hu, W. Chen, X. Xie, N. A. Liu, Y. Yang, H. Wu, Y. Yao, M. Pasta, H. N. Alshareef and Y. Cui, *ACS Nano*, 2011, **5**, 8904–8913.
15 L. B. Hu and Y. Cui, *Energy Environ. Sci.*, 2012, **5**, 6423–6435.

16 G. Y. Zheng, L. B. Hu, H. Wu, X. Xie and Y. Cui, *Energy Environ. Sci.*, 2011, **4**, 3368–3373.
17 Z. Weng, Y. Su, D. W. Wang, F. Li, J. Du and H. M. Cheng, *Adv. Energy Mater.*, 2011, **1**, 917–922.
18 G. Nystrom, A. Razaq, M. Stromme, L. Nyholm and A. Mihranyan, *Nano Lett.*, 2009, **9**, 3635–3639.
19 L. B. Hu, J. W. Choi, Y. Yang, S. Jeong, F. La Mantia, L. F. Cui and Y. Cui, *Proc. Natl. Acad. Sci. U. S. A.*, 2009, **106**, 21490–21494.
20 L. Y. Yuan, B. Yao, B. Hu, K. F. Huo, W. Chen and J. Zhou, *Energy Environ. Sci.*, 2013, **6**, 470–476.
21 M. Kaempgen, C. K. Chan, J. Ma, Y. Cui and G. Gruner, *Nano Lett.*, 2009, **9**, 1872–1876.
22 D. Pech, M. Brunet, H. Durou, P. Huang, V. Mochalin, Y. Gogotsi, P.-L. Taberna and P. Simon, *Nat. Nanotechnol.*, 2010, **5**, 651–654.
23 M. Q. Xue, F. W. Li, J. Zhu, H. Song, M. N. Zhang and T. B. Cao, *Adv. Funct. Mater.*, 2012, **22**, 1284–1290.
24 J. Chmiola, C. Largeot, P.-L. Taberna, P. Simon and Y. Gogotsi, *Science*, 2010, **328**, 480–483.
25 J. Lin, C. Zhang, Z. Yan, Y. Zhu, Z. Peng, R. H. Hauge, D. Natelson and J. M. Tour, *Nano Lett.*, 2012, **13**, 72–78.
26 W. Si, C. Yan, Y. Chen, S. Oswald, L. Han and O. G. Schmidt, *Energy Environ. Sci.*, 2013, **6**, 3218–3223.
27 J. T. Li, M. C. Lemme and M. Stling, *Adv. Mater.*, 2013, **25**, 3985–3992.
28 S. L. Wang, N. S. Liu, J. Y. Tao, C. X. Yang, W. J. Liu, Y. L. Shi, Y. M. Wang, J. Su, L. Y. Li and Y. H. Gao, *J. Mater. Chem. A*, 2015, **3**, 2407–2413.
29 G. Wee, T. Salim, Y. M. Lam, S. G. Mhaisalkar and M. Srinivasan, *Energy Environ. Sci.*, 2011, **4**, 413–416.
30 Y. Wang, Y. M. Shi, C. X. Zhao, J. I. Wong, X. W. Sun and H. Y. Yang, *Nanotechnology*, 2014, **25**, 094010–094017.
31 L. S. Fan, N. Q. Zhang and K. N. Sun, *Chem. Commun.*, 2014, **50**, 6789–6792.
32 N. Kurra, N. A. Alhebshi and H. N. Alshareef, *Adv. Energy Mater.*, 2015, **5**, 201401303.
33 B. S. Li, X. D. Wen, R. P. Li, Z. W. Wang, P. G. Clem and H. Y. Fan, *Nat. Commun.*, 2014, **5**, 4179–4185.
34 Y. J. Kang, H. Chung, C.-H. Han and W. Kim, *Nanotechnology*, 2012, **23**, 065401–065406.
35 T. Lindfors, Z. A. Boeva and R.-M. Latonen, *RSC Adv.*, 2014, **4**, 25279–25286.
36 N. Kurra, M. K. Hota and H. N. Alshareef, *Nano Energy*, 2015, **13**, 500–508.
37 E. Bekyarova, M. E. Itkis, N. Cabrera, B. Zhao, A. P. Yu, J. B. Gao and R. C. Haddon, *J. Am. Chem. Soc.*, 2005, **127**, 5990–5995.
38 E. Bekyarova, M. Davis, T. Burch, M. E. Itkis, B. Zhao, S. Sunshine and R. C. Haddon, *J. Phys. Chem. B*, 2004, **108**, 19717–19720.
39 L. L. Peng, X. Peng, B. R. Liu, C. Z. Wu, Y. Xie and G. H. Yu, *Nano Lett.*, 2013, **13**, 2151–2157.
40 L. Y. Yuan, X.-H. Lu, X. Xiao, T. Zhai, J. J. Dai, F. C. Zhang, B. Hu, X. Wang, L. Gong, J. Chen, C. G. Hu, Y. X. Tong, J. Zhou and Z. L. Wang, *ACS Nano*, 2012, **6**, 656–661.
41 M. Beidaghi and C. L. Wang, *Adv. Funct. Mater.*, 2012, **22**, 4501–4510.
42 F. S. Wen, C. X. Hao, J. Y. Xiang, L. M. Wang, H. Hou, Z. B. Su, W. T. Hu and Z. Y. Liu, *Carbon*, 2014, **75**, 236–243.
43 X. Xiao, T. Q. Li, P. H. Yang, Y. Gao, H. Y. Jin, W. J. Ni, W. H. Zhan, X. H. Zhang, Y. Z. Cao, J. W. Zhong, L. Gong, W.-C. Yen, W. J. Mai, J. Chen, K. F. Hou, Y.-L. Chueh, Z. L. Wang and J. Zhou, *ACS Nano*, 2012, **6**, 9200–9206.
44 T. M. Dinh, K. Armstrong, D. Guay and D. Pech, *J. Mater. Chem. A*, 2014, **2**, 7170–7174.
45 Y. P. Fu, X. Cai, H. W. Wu, Z. B. Lv, S. C. Hou, M. Peng, X. Yu and D. C. Zou, *Adv. Mater.*, 2012, **24**, 5713–5718.
46 L. Wei, M. Sevilla, A. B. Fuertes, R. Mokaya and G. Yushin, *Adv. Energy Mater.*, 2011, **1**, 356–361.
47 B. Yao, L. Y. Yuan, X. Xiao, J. Zhang, Y. Y. Qi, J. Zhou, J. Zhou, B. Hu and W. Chen, *Nano Energy*, 2013, **2**, 1071–1078.
48 D. Pech, M. Brunet, P. L. Taberna, P. Simon, N. Fabre, F. Mesnilgrente, V. Conedera and H. Durou, *J. Power Sources*, 2010, **195**, 1266–1269.
49 J.-X. Feng, S.-H. Ye, A.-L. Wang, X.-F. Lu, Y.-X. Tong and G.-R. Li, *Adv. Funct. Mater.*, 2014, **24**, 7093–7101.
50 Z. H. Wang, D. O. Carlsson, P. Tammel, K. Hua, P. Zhang, L. Nyholm and M. Strømme, *ACS Nano*, 2015, **9**, 7563–7571.

